


Tunicate cellulose nanocrystal reinforced polyacrylamide hydrogels with tunable mechanical performance

Kangwei Mo · Tiantian Zhang · Wei Yan · Chunyu Chang 

Received: 13 June 2018 / Accepted: 31 August 2018 / Published online: 10 September 2018
© Springer Nature B.V. 2018

Abstract Tunicate cellulose nanocrystals (TCNCs) are widely used as nanofillers for the reinforcements of polymeric materials because of their high aspect ratio and modulus. However, poor interfacial compatibility between TCNCs and polymer matrix always weakens the mechanical performance of nanocomposite materials. Herein, novel nanocomposite hydrogels composed of TCNCs and polyacrylamide (PAM) were generated by chemical crosslinking of PAM with TCNCs that worked as both multifunctional

crosslinkers and interfacial compatible nanofillers. Our strategy for the preparation of hydrogels avoided using any toxic crosslinking agent. The morphology, swelling behavior, and mechanical properties of nanocomposite hydrogels could be tuned by varying the amount of initiator. This work provided a simple, universal, and sustainable method to synthesize nanocomposite hydrogels with tunable mechanical performance.

K. Mo · W. Yan (✉)

Hubei Collaborative Innovation Center for Advanced Organic Chemical Materials, Ministry of Education, Key Laboratory of Green Preparation and Application for Functional Materials, Hubei Key Laboratory of Polymer Materials, School of Materials Science and Engineering, Hubei University, Wuhan 430062, China
e-mail: willieyancn2003@aliyun.com

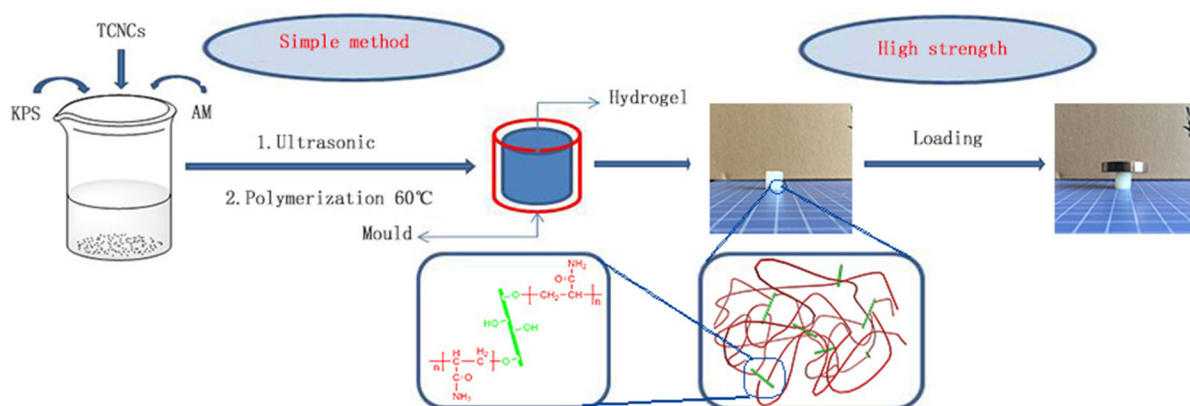
C. Chang (✉)

Suzhou Institute of Wuhan University, Wuhan University, Suzhou 215123, China
e-mail: changcy@whu.edu.cn;
changchunyu2001@163.com

K. Mo · T. Zhang · C. Chang

College of Chemistry and Molecular Sciences, Wuhan University, Wuhan 430072, China

Graphical abstract



Keywords Tunicate cellulose nanocrystals · Chemical crosslinking · High strength hydrogel · Polyacrylamide · Nanocomposite

Introduction

Hydrogels have a kind of three-dimensional network structure, which could absorb a mass of water. In the past two decades, hydrogels have been extensively studied because of their special properties such as biocompatibility, high swelling ratio, and bionic micro-environment (Chang et al. 2011; Peng et al. 2016; Zhang et al. 2017). Owing to their soft and wet properties, hydrogels have a very wide range of occasions can be used, including drug delivery (Hoare and Kohane 2008), tissue engineering (Hoffman 2012; Khademhosseini et al. 2009), biomolecular separation (Kim and Park 1998) and water treatment (Jing et al. 2013). However, the poor mechanical properties of conventional hydrogels seriously limited their practical applications, which have aroused much attention for scientists to develop hydrogels with improved mechanical properties. Nanocomposite hydrogels exhibited preferable mechanical performance after incorporating nanofillers into polymer matrix (Schexnailder and Schmidt 2009; Zhang and Shi 2011; Gulyuz and Okay 2014; Li et al. 2015). There are various kinds of nanofillers that could be employed to reinforce polymeric hydrogels, including silicate nanosheet, graphene, and nanoclay (Liu et al. 2006; Rao 2007; Xu et al. 2010; Cong et al. 2012; Haraguchi

et al. 2002). For example, Haraguchi et al. reported a series of nanoclay/polymer nanocomposite hydrogels with excellent stretch ability (Haraguchi and Li 2005; Haraguchi et al. 2006, 2011; Haraguchi 2007). Aida et al. used single layer of nano-titanium dioxide as photocatalytic cross-linking agent to fabricate photo-voltaic hydrogels (Liu et al. 2013).

Cellulose nanocrystals (CNCs) have attracted a great deal of interest in the nanocomposite field due to their appealing intrinsic properties such as nanoscale dimensions, high surface area, unique morphology, low density and mechanical strength (Habibi et al. 2010). Recently, a series of CNCs reinforced hydrogels have been reported by adjusting the interaction between CNCs and polymer matrix through controlling the crosslinking strategy (Yang et al. 2013, 2014, 2015; McKee et al. 2014; Chau et al. 2016). Compared with other CNCs, tunicate cellulose nanocrystals (TCNCs) isolated from the mantles of sessile sea creatures showed higher aspect ratio (> 70) (Sacui et al. 2014) and superior mechanical modulus (~ 140 GPa) (Sturcova et al. 2005). The characteristics of TCNCs facilitated the formation of rigid TCNC networks and improved the stress transfer efficiency, which improved the mechanical properties of nanocomposite materials (Capadona et al. 2008). On the other hand, TCNCs had a strong tendency for self-aggregation because of their highly interacting surface hydroxyl groups (De Souza Lima and Borsali 2004), leading to the limitation of mechanical reinforcing effect. Good dispersion of TCNCs in the polymer matrix could be achieved by surface modification of TCNCs to improve the interfacial

compatibility (Zhang et al. 2017). However, as far as we know, TCNCs reinforced hydrogels with completely chemically cross-linked networks have not been reported.

In this work, we attempted to design the hydrogels with tunable mechanical properties by using a facile method, where TCNCs worked as both nanofillers and multifunctional cross-linkers. Potassium persulfate was added into the mixture of TCNCs and acrylamide (AM) solution to initiate the radical polymerization of AM monomer and generate free radicals on the surface of TCNCs. AM monomers could bind to the surface of TCNCs and the molecular chain grew to form cross-linked hydrogel network. The morphology, swelling ratio, and mechanical property of nanocomposite hydrogels could be controlled by varying the amounts of initiator. This work proved a simple, fast, and universal way for the preparation of nanofiller reinforced nanocomposite hydrogels with chemically cross-linked networks.

Experimental

Materials

Tunicate (*Halocynthia roretzi* Drasche) was purchased from Weihai Evergreen Marine science and technology Co. Ltd (Shandong, China). Sulfuric acid, potassium persulfate (KPS), acrylamide (AM) was obtained from Sinopharm Chemical Reagent Co. Ltd. Other reagents were all analytical grade and all solutions were prepared with distilled water.

Isolation of tunicate cellulose nanocrystals (TCNCs)

Isolation of tunicate cellulose from *Halocynthia roretzi* Drasche was conducted according to our previous work (Zhang et al. 2017). 3 g tunicate cellulose were dispersed in sulfuric acid solution (300 mL, 65 wt%), and stirred at speed of 300 rpm at 60 °C for 6 h. For the removal of large particles and remaining sulfuric acid, the mixture was centrifuged at 7500 rpm, then diluted with water, and dialyzed with water until neutral.

Synthesis of TCNC/PAM hydrogels

For the preparation of TCNC/PAM hydrogels, 1 g AM, 2.8 g TCNC suspension (2.83 wt%), and a certain amount of KPS were added into distilled water to obtain 5 g mixture. Then, the mixture was treated with ultrasound in ice-water bath for 10 min and poured into the mold to react 3 h at 60 °C. Finally, TCNC/PAM hydrogels were carefully taken out and immersed in distilled water to remove excess monomers and initiators. The as-prepared hydrogels were coded as Gel-0.04, Gel-0.2, Gel-0.4, Gel-1, Gel-2, and Gel-4, according to KPS concentration of 0.04 wt%, 0.2 wt%, 0.4 wt%, 1 wt%, 2 wt%, and 4 wt%, respectively. The content of TCNCs was controlled to be 7.34 wt% in the dried gel.

Characterization

Transmission electron microscope (TEM) observation of TCNCs was performed by using a JEM-2010 transmission electron microscope (JEOL, Japan) with an acceleration voltage at 200 kV, where a droplet of dilute TCNC suspension (0.01 wt%) was dropped and dried on a copper grid before measurement. Fourier transfer infrared spectroscopy (FTIR) was carried out by NICOLET 5700 FTIR spectrometer (Thermo Fisher Scientific, USA). Scanning electron microscope (SEM) images were taken with the field emission scanning electron microscopy (FESEM, Zeiss, Germany) at an accelerating voltage of 5 kV. The hydrogels were swollen to equilibrium in distilled water, frozen in liquid nitrogen, snapped immediately, and freeze-dried at -40 °C. Cross-section of specimens was coated with gold vapor, observed, and photographed. Zeta potential was measured by ZetaSizer Nano series Nano-ZS (Malvern Instruments Ltd, Malvern, UK) at room temperature. The mechanical properties of hydrogels were tested at room temperature by using a universal testing machine (CMT6350, Shenzhen SANS, China). For tensile test, the size of rectangular samples were 30 mm (L) \times 8 mm (W) \times 1 mm (T), the crosshead speed was 20 mm min⁻¹, and the initial length of the hydrogel samples for tensile test between two clamps was 20 mm. For the compression test, the dimension of cylinder samples was about 9 mm (D) \times 6.5 mm (H), the crosshead speed was 0.5 mm min⁻¹, and the initial height of the hydrogel samples for compressive

test between two clamps was 6.5 mm. As for the loading–unloading tests, the final strains were fixed to be 250% and 70% for tensile and compressive tests, respectively. The swelling ratio of hydrogel was measured by gravimetric method. The SR value was calculated as follows.

$$\text{Swelling Ratio} = \frac{W_t - W_d}{W_d} \quad (1)$$

where W_t is the weight of swollen hydrogel at time t and W_d is the weight dried gel.

Results and discussion

Preparation, structure, and morphology of TCNC/PAM hydrogel

Owing to the presence of negatively charged sulfonate groups on their surface, TCNCs could be well dispersed in the suspension benefiting from the electrostatic repulsion. Figure 1 shows the TEM image and size distribution of TCNCs. It can be seen that TCNCs exhibited strips-like morphology with average length of 1880 ± 57 nm and average diameter of 26 ± 11 nm. The aspect ratio of TCNCs was calculated to be ~ 72 , which was consistent with the reported value (Cheng et al. 2018). The zeta potential of TCNCs was -30.6 mV, confirming the negatively charged surface of TCNCs. For the fabrication of nanocomposite hydrogels, TCNC suspension, AM monomer, and initiator were uniformly blended to obtain mixture. Then, temperature was raised to 60 °C for conducting polymerization and crosslinking (Fig. 2). The initiator (KPS) could initiate polymerization of AM monomer, while radicals were generated on the surface of TCNCs by oxidizing the

hydroxyl groups with KPS, which could react with AM monomers to form chemically cross-linked network. Therefore, the density of hydrogel network could be controlled by altering the amount of KPS. For example, low usage of KPS resulted in long PAM chains and lightly cross-linked hydrogel. In contrast, heavily cross-linked hydrogel would be produced by using more initiator.

The chemical structure of TCNC/PAM hydrogels was characterized by FTIR, as shown in Fig. 3. Compared with the spectrum of PAM, the characteristic peak at 3440 cm^{-1} which belongs to $-\text{OH}$ and $-\text{NH}_2$ stretching vibration became wider in the spectra of Gel-0.4 and Gel-4. These results revealed that strong hydrogen bonds formed between the amino groups of PAM and hydroxyl groups of TCNCs in the hydrogel network. Importantly, the peak appeared at 1060 cm^{-1} could not be found in the spectrum of PAM, but it was available in the spectrum of TCNCs, which could be attributed to the absorption peak of $\text{C}-\text{O}-\text{C}$. In the spectra of nanocomposite hydrogels, the intensity of the peak at 1060 cm^{-1} sharply increased when TCNCs content was higher. It indicated that the covalent bonds formed between AM monomers and TCNCs, and hydrogel network was successfully constructed.

The morphologies of TCNC/PAM hydrogels were characterized by using SEM technology. Figure 4 shows the SEM images of nanocomposite hydrogels. All hydrogels exhibited porous structure, where the pore size of samples gradually reduced as the increase of initiator concentration. For example, Gel-0.04 had macroporous morphology with the average pore size of 13 μm . When the concentration of KPS increased to 4 wt%, the pore size of Gel-4 was only ~ 1 μm . These results indicated that the crosslinking density of

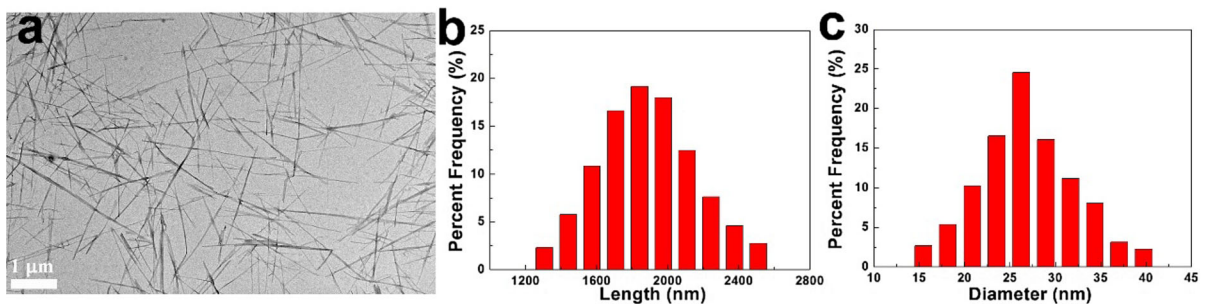


Fig. 1 TEM image (a) and size distribution (b, c) of TCNCs

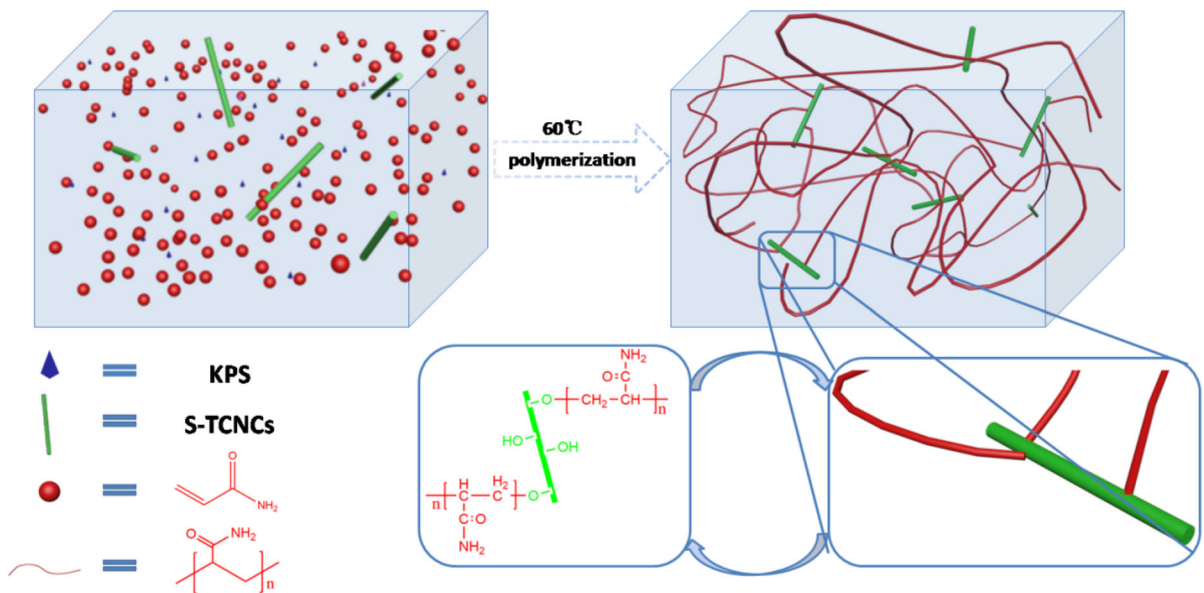


Fig. 2 Schematic illustration for the formation of TCNC/PAM hydrogel

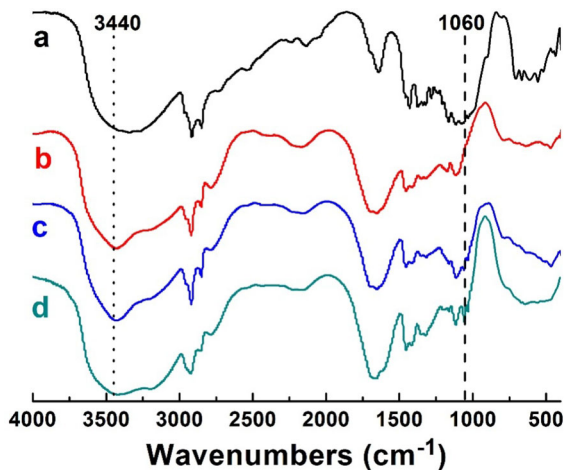


Fig. 3 FTIR spectra of TCNCs, PAM hydrogel, and TCNC/PAM hydrogels: (a) TCNCs, (b) PAM, (c) Gel-0.4, and (d) Gel-4

hydrogel network could be significantly improved by raising the KPS concentration.

Mechanical property and swelling behavior of TCNC/PAM hydrogel

The appearances of TCNC/PAM hydrogels are shown in Fig. 5. To compare the mechanical properties of hydrogels, the water contents of all hydrogel samples were controlled to 80 wt%. All hydrogels were opaque, due to the phase separation in the hydrogel networks, as shown in Fig. 5a. Despite the similar appearances of hydrogel samples, their mechanical performances were quite different. After loading a piece of iron slab on the hydrogels, Gel-0.04 largely deformed because of its soft nature, but Gel-4 was stiff and hard enough to tolerate the loading without

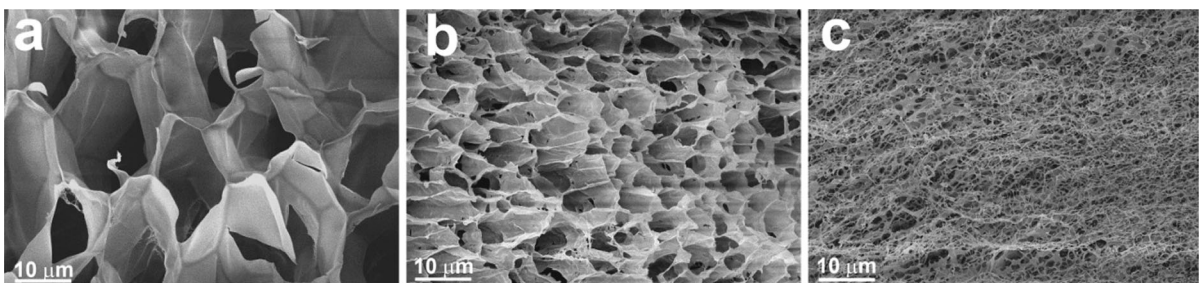


Fig. 4 SEM images of TCNC/PAM hydrogels: a Gel-0.04, b Gel-0.4, and c Gel-4

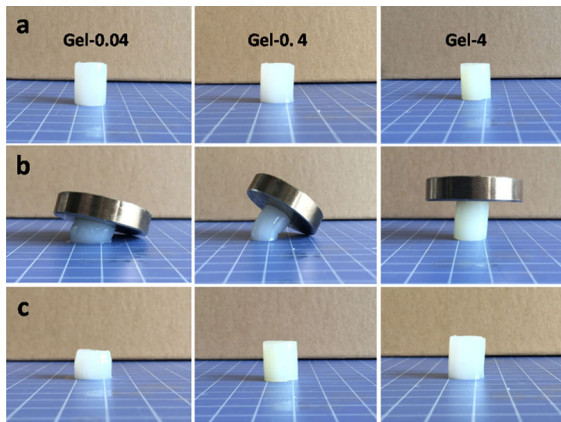


Fig. 5 Photographs of TCNC/PAM hydrogels before (a) and after loading iron slabs (b, c)

apparent deformation (Fig. 5b). When the iron slab was removed, the deformed Gel-0.04 could not recover (Fig. 5c), revealing that the chemically cross-linked network of hydrogel was irreversibly destroyed by external force. These results suggested that the mechanical performances of hydrogels could be tuned by varying the concentration of KPS.

To quantitatively investigate the mechanical property of hydrogels, both tensile and compressive tests have been conducted for all samples with water content of $\sim 80\%$. The tensile stress–strain curves of nanocomposite hydrogels are shown in Fig. 6a. The mechanical performances of hydrogel samples were strongly dependent on the initiator concentration in the preparation process. As the concentration of initiator increased, the tensile strength of hydrogel samples

gradually increased from 62.5 to 501.5 kPa, whereas the fracture strain decreased from 1527 to 124%. By adjusting the concentration of KPS, soft and stretchable Gel-0.04 converted to strong and stiff Gel-4, revealing that the mechanical property of hydrogel samples were tunable. Moreover, the elastic modulus and toughness of various nanocomposite hydrogels are shown in Fig. 6b. The elastic modulus of hydrogel samples gradually increased with the concentration of KPS from 20 to 483 kPa. This result suggested that the improvement of the crosslinking density of hydrogel network could effectively enhanced the stiffness of hydrogels. However, toughness of nanocomposite hydrogels increased first and then decreased along with the raise of KPS concentration (Fig. 6b). Despite higher KPS concentration could improve the tensile stress of nanocomposite hydrogels, their fracture strain sharply decreased, resulting in the decline of toughness. Therefore, the maximal value of toughness was 964.5 kJ m^{-3} as the concentration of initiator was 0.4 wt%.

The compressive tests had similar tendency to the result of tensile measurement, where the mechanical properties of the hydrogel strongly depend on initiator concentration. The compressive stress–strain curves of various TCNC/PAM hydrogels are shown in Fig. 7a. As the dosage of initiator in the samples increased, the compressive stress increased from 0.18 MPa for G-0.04 to 2.46 MPa for G-4. On the other hand, the elastic modulus of TCNC/PAM hydrogels samples gradually increased from 1.83 to 11.53 MPa (Fig. 7b) with the increase of KPS concentration from 0.04 to 4 wt%, indicating that

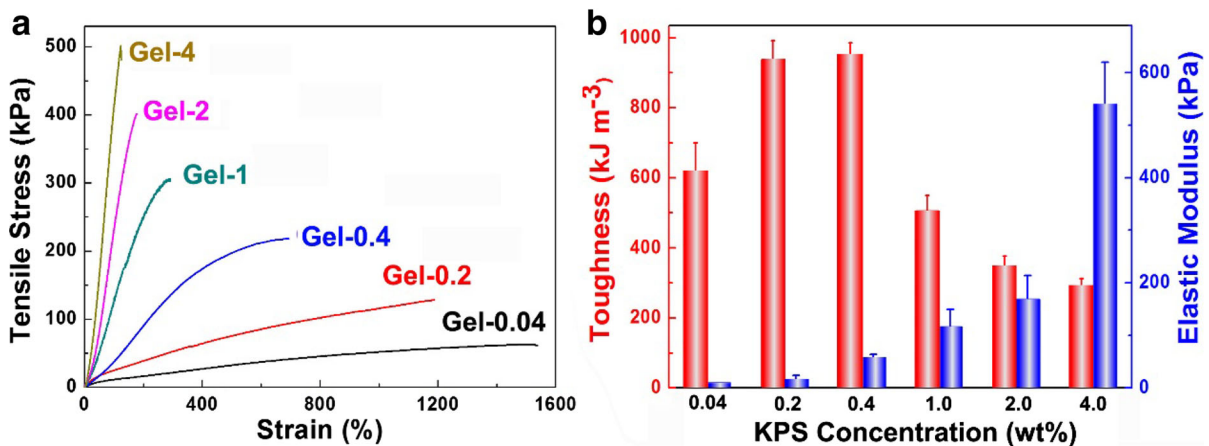


Fig. 6 Stress–strain curves (a), and corresponding statistics toughness and elastic modulus (b) of various TCNC/PAM hydrogels

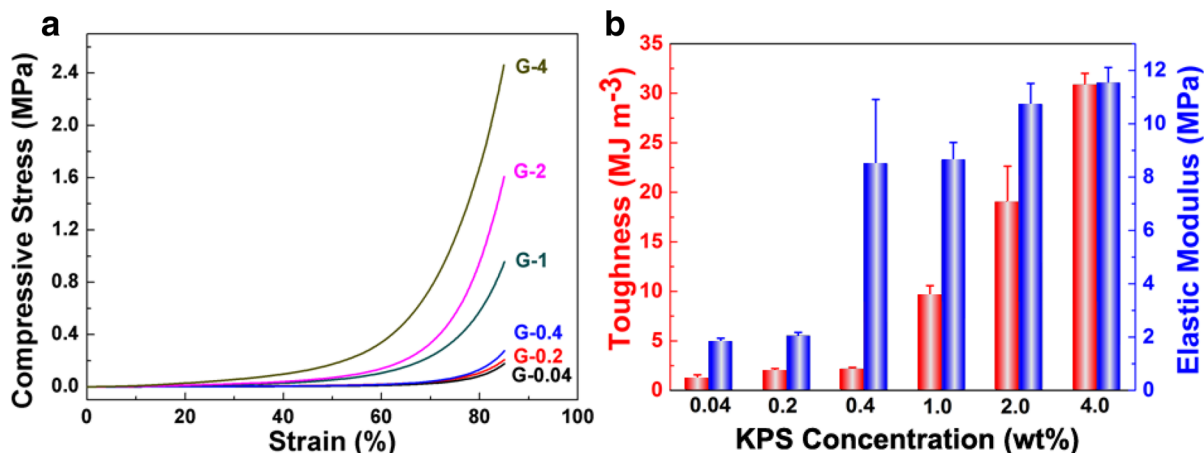


Fig. 7 Compressive stress–strain curves (a), and corresponding statistics elastic modulus (b) of various TCNC/PAM hydrogels

hydrogel samples behaved stiffer with higher initiator concentration. These results suggested that crosslinking density of hydrogel networks could be tailored by varying initiator concentration, resulting in tunable mechanical properties of TCNC/PAM hydrogels.

To better understand the dissipation of mechanical energy, the repeated loading–unloading tensile and compressive tests of TCNC/PAM hydrogels were conducted. For successive tensile tests, the dissipated mechanical energy was about 7.85 kJ m^{-3} in the first loading–unloading cycle, which decreased to $1.41\text{--}1.15 \text{ kJ m}^{-3}$ in the 2–5th cycles (Fig. 8a). These results indicated that the hydrogel sample was mainly consisted by chemically cross-linked networks which were damaged to dissipate most of energy in the first

loading–unloading cycle. Moreover, the successive compressive curves of G-4 during 5 loading–unloading cycles with a strain of 70% is shown in Fig. 8b. The dissipated mechanical energy calculated from the area of hysteresis loop was 4.48 MJ m^{-3} for the 1st cycle, which reduced to 1.42 MJ m^{-3} for the 2nd cycle. Finally, the dissipated energy maintained at 1.2 MJ m^{-3} in the 3–5th cycles. These results revealed that the chemical crosslinking was broken during the initial cycle resulting in dissipating mechanical energy and the reversible physical interaction existed in the 2–5th cycles.

To investigate the swelling kinetics of TCNC/PAM hydrogels, the dried gels were immersed in distilled water at $25 \text{ }^\circ\text{C}$ (Fig. 9a). Four hydrogel samples

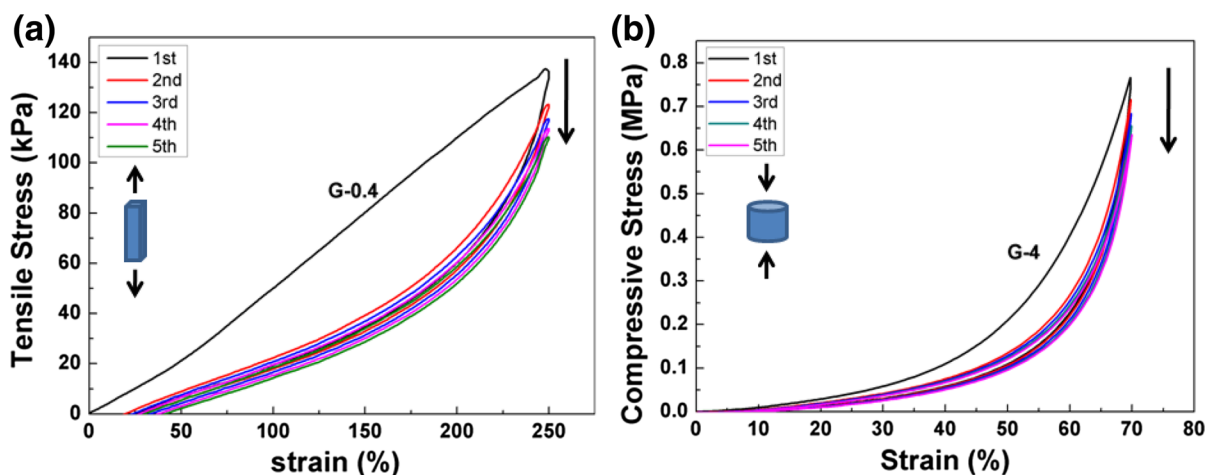


Fig. 8 Successive tensile curves of G-0.4 sample during 5 times loading–unloading cycles with a strain of 250% (a), and successive compressive curves of G-4 sample during 5 times loading–unloading cycles with a strain of 70% (b)

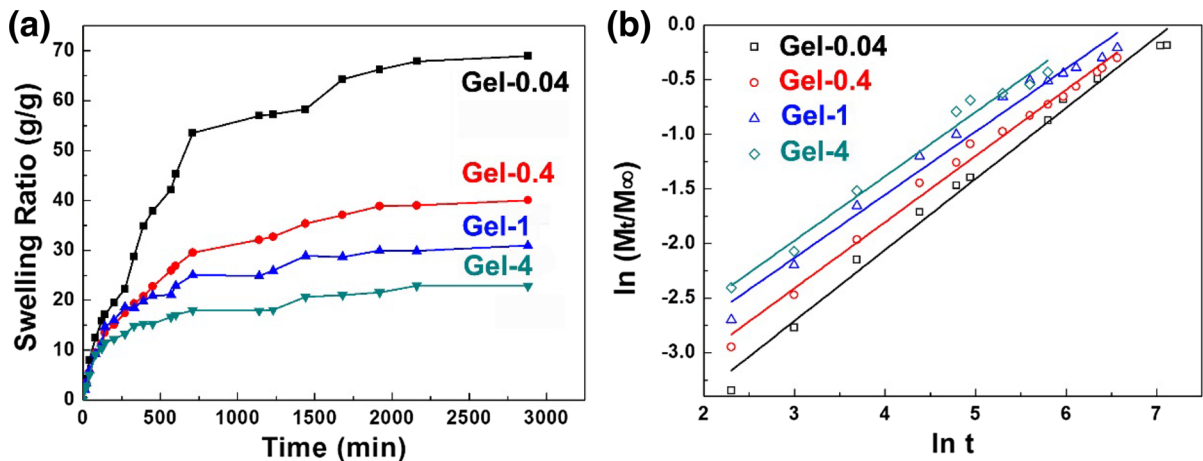


Fig. 9 Swelling kinetics of various TCNC/PAM hydrogels in distilled water at 25 °C (a), and plots of $\ln(M_t/M_\infty)$ against $\ln t$ (b)

Table 1 Diffusion characteristic of hydrogels in distilled water at 25 °C

Samples	Diffusional exponent n	Diffusional constant k	Correlation coefficient r
Gel-0.04	0.650	0.0095	0.988
Gel-0.4	0.606	0.0146	0.991
Gel-1	0.577	0.0210	0.979
Gel-4	0.588	0.0238	0.980

exhibited similar swelling tendency, where the swelling ratio of dried samples increased rapidly at initial stage and then the swelling rate gradually slowed down until equilibrium. The equilibrium swelling ratio of hydrogel samples decreased as the increase of the KPS usage. For example, the equilibrium swelling ratio of Gel-0.04 was 69 g g^{-1} , but that of Gel-4 decreased to 23 g g^{-1} . These results were attributed to the difference in crosslinking density of hydrogel samples, which were in good agreement with SEM results. Furthermore, the following exponential Eq. (2) was used to determine the diffusion mechanism of water into hydrogel samples.

$$\frac{M_t}{M_\infty} = kt^n \quad (2)$$

where M_t and M_∞ were the amount of water diffused into the gel at time t , and infinite time (equilibrium), respectively. k was a diffusion coefficient which was relative with structure of the network. The exponent n was the diffusion index which could be used to determine the type of diffusion. For cylindrical samples, $n \leq 0.5$ indicated that the diffusion was

Fickian diffusion, but $0.5 < n < 1.0$ represented non-Fickian diffusion (Zhou et al. 2007; Franson and Peppas 1983). For TCNC/PAM hydrogels, we calculated the exponent n and diffusion coefficient k from the slope and intercept of straight line in Fig. 9b. The n values of TCNC/PAM hydrogels were 0.650, 0.606, 0.577, and 0.588, for Gel-0.04, Gel-0.4, Gel-1, and Gel-4, respectively (Table 1), revealing non-Fickian diffusion character. In the non-Fickian diffusion, initial water absorption in the dried gel was controlled collaboratively by water diffusion and relaxation of polymer chains (Lee et al. 2018). Therefore, the crosslinking density of hydrogel samples increased as the increase of KPS concentration from Gel-0.04 to Gel-4, which gradually limited the movability of polymer chains, leading to the decline of n values.

Conclusion

We have successfully designed and fabricated a series of TCNC/PAM nanocomposite hydrogels. TCNCs acted as multifunctional crosslinking agents and

nanofillers in the hydrogel network. Both the hydroxyl groups on the surface of TCNCs and AM monomers were oxidized and triggered by initiator to generate free radicals, resulting in the growth of polymer chains and the formation of chemical bonds between PAM and TCNCs. The morphology, mechanical performance and swelling behavior of nanocomposite hydrogels could be well controlled by altering the amounts of initiator. This work provided a simple, rapid, and universal method for the synthesis of mechanically tunable nanocomposite hydrogels.

Acknowledgments This work was supported by the National Natural Science Foundation of China (51873164 and 21304021), Jiangsu Province Science Foundation for Youths (BK20150382), Pearl River S&T Nova Program of Guangzhou (201506010101), State Key Laboratory of Pulp and Paper Engineering (201824), and the Fundamental Research Funds for the Central Universities (2042018kf0213 and 2042015kf0028).

References

- Capadona JR, Shanmuganathan K, Tyler DJ, Rowan SJ, Weder C (2008) Stimuli-responsive polymer nanocomposites inspired by the sea cucumber dermis. *Science* 319:1370–1374
- Chang C, Zhang L, Chen S (2011) Novel hydrogels prepared via direct dissolution of chitin at low temperature: structure and biocompatibility. *J Mater Chem* 21:3865–3871
- Chau M, France KJD, Kopera B et al (2016) Composite hydrogels with tunable anisotropic morphologies and mechanical properties. *Chem Mater* 28:3406–3415
- Cheng Q, Ye D, Yang W, Zhang S, Chen H, Chang C, Zhang L (2018) Construction of transparent cellulose-based nanocomposite papers and potential application in flexible solar cells. *ACS Sustain Chem Eng* 6:8040–8047
- Cong H, Ren X, Wang P, Yu S (2012) Macroscopic multifunctional graphene-based hydrogels and aero gels by a metal ion induced self-assembly process. *ACS Nano* 6:2693–2703
- De Souza Lima MM, Borsali R (2004) Rod like cellulose microcrystals: structure, properties, and applications. *Macromol Rapid Commun* 25:771–787
- Franson NM, Peppas NA (1983) Influence of copolymer composition on non-fickian water transport through glassy copolymers. *J Appl Polym Sci* 28:1299–1310
- Gulyuz U, Okay O (2014) Self-healing poly(acrylic acid) hydrogels with shapememory behavior of high mechanical strength. *Macromolecules* 47:6889–6899
- Habibi Y, Lucia LA, Rojas OJ (2010) Cellulose nanocrystals: chemistry, self-assembly, and applications. *Chem Rev* 110:3479–3500
- Haraguchi K (2007) Nanocomposite hydrogels. *Curr Opin Solid State Mater Sci* 11:47–54
- Haraguchi K, Li H (2005) Control of the coil-to-globule transition and ultra-high mechanical properties of PNIPA in nanocomposite hydrogels. *Angew Chem Int Ed* 44:6500–6504
- Haraguchi K, Takehisa T, Fan S (2002) Effects of clay content on the properties of nanocomposite hydrogels composed of poly(*N*-isopropyl AM) and clay. *Macromolecules* 35:10162–10171
- Haraguchi K, Ebato M, Takehisa T (2006) Polymer-clay nanocomposites exhibiting abnormal necking phenomena accompanied by extremely large reversible elongations and excellent transparency. *Adv Mater* 18:2250–2254
- Haraguchi K, Uyama K, Tanimoto H (2011) Self-healing in nanocomposite hydrogels. *Macromol Rapid Commun* 32:1253–1258
- Hoare TR, Kohane DS (2008) Hydrogels in drug delivery: progress and challenges. *Polymer* 49:1993–2007
- Hoffman AS (2012) Hydrogels for biomedical applications. *Adv Drug Deliv Rev* 64:18–23
- Jing G, Wang L, Yu H et al (2013) Recent progress on study of hybrid hydrogels for water treatment. *Colloids Surf A* 416:86–94
- Khademhosseini A, Vacanti JP, Langer R (2009) Progress in tissue engineering. *Sci Am* 300:64–71
- Kim JJ, Park K (1998) Smart hydrogels for bioseparation. *Bioseparation* 7:177–184
- Lee J, Park S, Roh H, Oh S, Kim S, Kim M, Kim D, Park J (2018) Preparation and characterization of superabsorbent polymers based on starch aldehydes and carboxymethyl cellulose. *Polymers* 10:605
- Li Y, Chen H, Liu D et al (2015) pH-responsive shape memory poly(ethyleneglycol)-poly(ϵ -caprolactone)-based polyurethane/cellulose nanocrystals nanocomposite. *ACS Appl Mater Interfaces* 7:12988–12999
- Liu Y, Zhu M, Liu X et al (2006) High clay content nanocomposite hydrogels with surprising mechanical strength and interesting deswelling kinetics. *Polymer* 47:1–5
- Liu M, Ishida Y, Ebina Y et al (2013) Photolatently modulable hydrogels using unilamellar titania nanosheets as photocatalytic crosslinkers. *Nat Commun* 4:2029
- McKee JR, Appel EA, Seitonen J et al (2014) Healable, stable and stiff hydrogels: combining conflicting properties using dynamic and selective three-component recognition with reinforcing cellulose nanorods. *Adv Funct Mater* 24:2706–2713
- Peng N, Hu D, Zeng J, Li Y, Liang L, Chang C (2016) Superabsorbent cellulose-clay nanocomposite hydrogels for highly efficient removal of dye in water. *ACS Sustain Chem Eng* 4:7217–7224
- Rao YQ (2007) Gelatin-clay nanocomposites of improved properties. *Polymer* 48:5369–5375
- Sacui IA, Nieuwendaal RC, Burnett DJ, Stranick SJ, Jorfi M, Weder C, Foster EJ, Olsson RT, Gilman JW (2014) Comparison of the properties of cellulose nanocrystals and cellulose nanofibrils isolated from bacteria, tunicate, and wood processed using acid, enzymatic, mechanical, and oxidative methods. *ACS Appl Mater Interfaces* 6:6127–6138
- Schexnailder P, Schmidt G (2009) Nanocomposite polymer hydrogels. *Colloid Polym Sci* 287:1–11
- Sturcova A, Davies GR, Eichhorn SJ (2005) Elastic modulus and stress-transfer properties of tunicate cellulose whiskers. *Biomacromol* 6:1055–1061

- Xu Y, Wu Q, Sun Y et al (2010) Three-dimensional self-assembly of graphene oxide and DNA into multifunctional hydrogels. *ACS Nano* 4:7358–7362
- Yang J, Zhao JJ, Xu F et al (2013) Revealing strong nanocomposite hydrogels reinforced by cellulose nanocrystals: insight into morphologies and interactions. *ACS Appl Mater Interfaces* 5:12960–12967
- Yang J, Zhao JJ, Han CR et al (2014) Tough nanocomposite hydrogels from cellulose nanocrystals/poly(AM) clusters: influence of the charge density, aspect ratio and surface coating with PEG. *Cellulose* 21:541–551
- Yang J, Zhang X, Xu F (2015) Design of cellulose nanocrystals template-assisted composite hydrogels: insights from static to dynamic alignment. *Macromolecules* 48:1231–1239
- Zhang L, Shi G (2011) Preparation of highly conductive graphene hydrogels for fabricating super capacitors with high rate capability. *J Phys Chem C* 115:17206–17212
- Zhang T, Cheng Q, Ye D, Chang C (2017) Tunicate cellulose nanocrystals reinforced nanocomposite hydrogels comprised by hybrid cross-linked networks. *Carbohydr Polym* 169:139–148
- Zhou J, Chang C, Zhang R, Zhang L (2007) Hydrogels prepared from unsubstituted cellulose in NaOH/urea aqueous solution. *Macromol Biosci* 7:804–809